Chapter 4
The Laegeren Site: An Augmented Forest Laboratory

Combining 3-D Reconstruction and Radiative Transfer Models for Trait-Based Assessment of Functional Diversity

Felix Morsdorf, Fabian D. Schneider, Carla Gullien, Daniel Kükenbrink, Reik Leiterer, and Michael E. Schaepman

4.1 Introduction

Global change is altering biodiversity in an unprecedented manner (Parmesan and Yohe 2003), and its impact on humankind may be large (Chapin III et al. 2000; Isbell et al. 2017). Forests are of special relevance because they hold most of the terrestrial biomass (Bar-On et al. 2018), are a hot spot of biodiversity (Wilson et al. 2012), and are subject to climate- and human-induced changes (Gardner 2010; Hansen et al. 2013). To monitor and potentially mitigate changes in biodiversity, Pereira et al. (2013) defined a set of essential biodiversity variables (EBVs), which should be comprehensive, concise, and standardized. Originally, most of these EBVs were to be measured in situ within ecosystems, but because forest plots are particularly scarce in the regions where change is happening the fastest (Chave et al. 2014), remote sensing (RS) has been acknowledged as a vital component to contribute to the aims of EBVs in the form of RS-enabled EBVs (RS-EBVs; Pettorelli et al. 2016; O'Connor et al. 2015). More specifically, RS technologies such as imaging spectroscopy and laser scanning have been attributed with the potential to play an important role in providing the necessary information for RS-EBVs, be it at regional, national, or global scale (Skidmore et al. 2015; Jetz et al. 2016).

Still in its early stage is the design and use of the EBV framework to include and combine RS-EBVs with in-situ measurements. In-situ measurements are often based on point measurements of individual species, whereas RS-EBVs are area-

F. Morsdorf (✉) · F. D. Schneider · C. Gullien · D. Kükenbrink · R. Leiterer · M. E. Schaepman
Remote Sensing Laboratories, Department of Geography, University of Zurich, Zurich, Switzerland
e-mail: felix.morsdorf@geo.uzh.ch

J. Cavender-Bares et al. (eds.), *Remote Sensing of Plant Biodiversity*,
https://doi.org/10.1007/978-3-030-33157-3_4

based, with spatial characteristics depending on sensor resolution and coverage, similar to the concept of grain and extent in ecology (Turner 1989).

For large-scale assessments (i.e., regional, continental, global), cost and effort of fieldwork is a limiting factor with respect to in-situ observations. Data from the newest generation of optical satellites (e.g., Landsat 8 and Sentinel-2) have high potential for a global biodiversity assessment due to their high spatial resolution (10–30 m), multispectral information, and temporal coverage, with repeat passes within 5–6 days, depending on the area of interest. Nevertheless, due to their recent launch, these sensors do not provide a long time series, and the complementarity of lower resolution satellite data or airborne or terrestrial RS data in combination with in-situ observation is beneficial to map changes at decadal or longer timescales.

All optical RS approaches use reflected light of the vegetation canopy to infer information about its state (Schaepman et al. 2009; Homolová et al. 2013). Leaf-level biochemistry (e.g., traits such as chlorophyll and water content) has strong links with leaf reflectance and transmittance (Jacquemoud and Baret 1990). However, when light interacts with the canopy, a multitude of scattering and absorption processes have to be considered (North 1996), taking place at different levels (e.g., leaf, tree, canopy; Niinemets et al. 1998) of the canopy. Thus, passive optical observational approaches of forested ecosystems are susceptible to the effects of forest structure because directional effects associated with illumination and observation geometry may interact with signals related to leaf-level biochemistry (Hilker et al. 2008; Knyazikhin et al. 2013). Consequently, the reflectance signal at the canopy level is influenced by both vegetation structure and leaf-level physiology, and disentangling those based on passive optical data alone remains a difficult problem (Kotz et al. 2004). The effect of vegetation structure on RS indices and products (e.g., RS-EBVs) is difficult to assess, and its impact on current observations and predictions may be large. The validation of advanced wall-to-wall RS products becomes increasingly difficult because of spatiotemporal mismatches of in-situ observations with RS data. Hence, we need a framework to be able to upscale and validate leaf-level physiological traits to the level of RS data to test potential observables for RS-informed EBVs.

Radiative transfer (RT) modeling has been used for several decades to simulate and understand the signals in passive optical data (Myneni et al. 1995, 1997; Meroni et al. 2004; Lewis and Disney 2007; Gastellu-Etchegorry et al. 1996). In addition, RT models (RTMs) have been used with existing medium- to low-resolution spaceborne missions for the retrieval of products such as leaf area index (LAI) or fraction of absorbed photosynthetic radiation (fAPAR) through inversion (Myneni et al. 1997; Running et al. 2004). One particular issue with RTMs of vegetation is their parameterization. While modeling approaches simulating low-resolution data [such as Moderate Resolution Imaging Spectroradiometer (MODIS) or MEdium Resolution Imaging Spectrometer (MERIS)] mainly used one-dimensional parameterizations of the vegetation (Jacquemoud 1993; Huemmrich 2001; Verhoef and Bach 2007), higher-resolution sensors will need 3-D parameterization to account for effects like shadowing and multiple scattering (Asner and Warner 2003; Disney et al. 2006; Widlowski et al. 2015). The first RTMs incorporating 3-D forest structure were called geometric-optical radiative transfer (GORT)-type models (Ni et al. 1999).

While they were better at modeling directional effects than 1-D models, they still lacked multiple scattering and did not have full energy balance closure of incoming and outgoing radiation across all spectral domains. More advanced models use Monte Carlo ray tracing (MCRT) to add multiple scattering and provide a sound physical representation of the photon's interaction with vegetation canopies (Disney et al. 2006). While the inclusion of more physical processes (e.g., multiple scattering) certainly improves MCRT-type models over simpler approaches, their parameterization and benchmarking remains an issue. A large effort in testing RT models was undertaken in the course of the radiation transfer modeling intercomparison (RAMI) exercise, where different models were tested using a set of artificial scenes of different complexity, including 3-D scenes, to see if the models produced comparable results (Widlowski et al. 2008, 2015). However, this benchmarking remained relative (i.e., representing actual forest patches that could be validated with real-world Earth observation (EO) data acquired over the same area was not an aim of the RAMI exercise). One reason, among others, for this was the lack of suitable technologies and methods to capture and represent the 3-D vegetation structure at small scales (e.g., branches, leaves, and/or shoots).

Today, laser scanning is an established tool for retrieving quantitative measures of canopy structure (Nelson 1997; Lefsky et al. 1999; Næsset 2002; Morsdorf et al. 2004; Popescu et al. 2002; Morsdorf et al. 2006, 2010; Nelson 2013; Wulder et al. 2012). Airborne (ALS)-, terrestrial (TLS)-, and unmanned aerial vehicle (UAV)-based laser scanning (Morsdorf et al. 2017) provide a direct means to assess vegetation structure by combining the known position and orientation of the sensor with the time of flight of a laser pulse to produce a point cloud of exact 3-D coordinates. Measurements can be made across scales (e.g., stand, tree, branch, and leaf level) with finer scales often captured by close-range laser scanning (Morsdorf et al. 2018). The amount of structural detail contained in the point cloud can be overwhelming, and the extraction of meaningful information remains a challenge (Wulder et al. 2013; Morsdorf et al. 2018). Due to large data sets, automated methods for the extraction of either semantic information, such as single-tree detection based on ALS (Hyyppa et al. 2001; Morsdorf et al. 2004; Kaartinen et al. 2012; Wang et al. 2016) or tree geometry reconstruction from TLS (Cote et al. 2009; Raumonen et al. 2013) or the derivation of biophysical variables such as LAI (Morsdorf et al. 2006), are preferable over manual and/or empirical approaches.

Figure 4.1 shows an example of a single-tree-based 3-D reconstruction using ALS- and TLS-derived information. Using the 3-D information derived by ALS and TLS, one can reconstruct a virtual representation of the forest that will be used by the RT model to simulate the radiative regime of the canopy. Such an approach can be utilized to upscale measurements of leaf biochemistry to the canopy scale and to validate imaging spectroscopy-derived RS-EBVs across larger regions. In addition, this approach uses a set of three physiological and tree morphological functional traits, derived from imaging spectroscopy and laser scanning, respectively, to showcase the potential of these technologies to map the functional diversity of forests and to provide relevant information for RS-enabled EBVs.

Here we describe how we (i) designed and implemented an observational scheme to gather in-situ and structural data across several scales to simulate the 3-D radiative

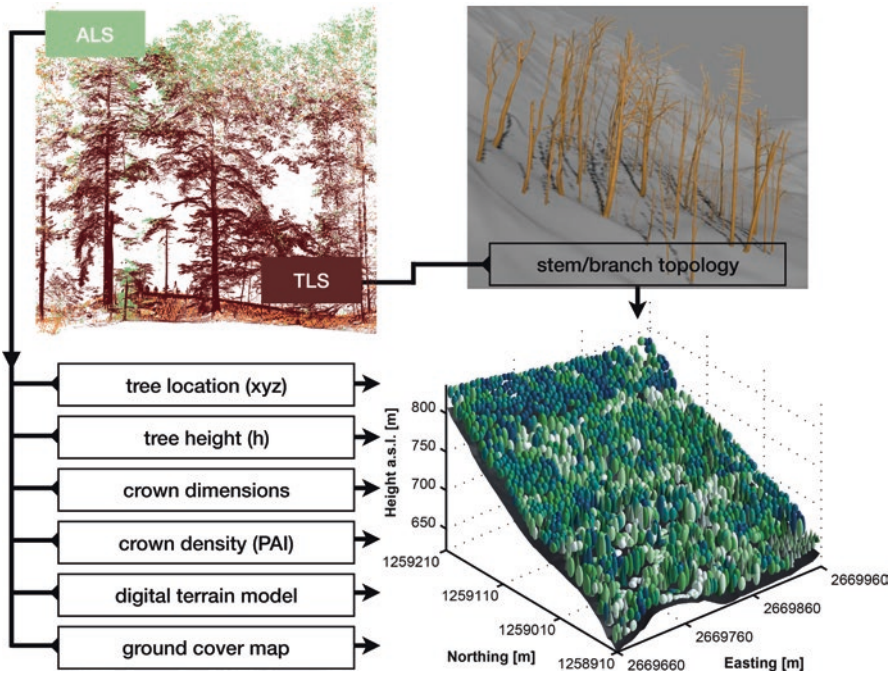

Fig. 4.1 Workflow of the 3-D reconstruction using ALS and TLS measurements

regime of the forest, (ii) tested the simulation by comparing simulated and actual RS data in their spectral and spatial information dimension, and (iii) use the approach to demonstrate how remotely sensed functional traits can be used to compute regional-scale functional richness, showcasing the information content of RS-EBVs.

4.2 The Laegeren Site: Description and History

The Laegeren site is located at N 47° 28′, 49″ and E 8° 21′, 05″ at 680 m a.s.l. on the southern slope of the Laegeren mountain, approximately 15 km northwest of Zürich, Switzerland (Fig. 4.2). The southern slope of the Laegeren marks the boundary of the Swiss Plateau, which is bordered by the Jura and the Alps. Since 1986, a 45-m-tall flux tower has provided micrometeorological data at high temporal resolution. Since April 2004, CO_2 and H_2O flux measurements are a routinely contribution to the FLUXNET/CarboEurope-IP network (Eugster et al. 2007). The mean annual temperature is 8°C. The mean annual precipitation is 1200 mm, and the growing season lasts 170–190 days. The natural vegetation cover around the tower is a mixed beech forest. The western part is dominated by broad-leaved trees, mainly beech (*Fagus sylvatica L.*) and ash (*Fraxinus excelsior L.*). In the eastern part, beech and

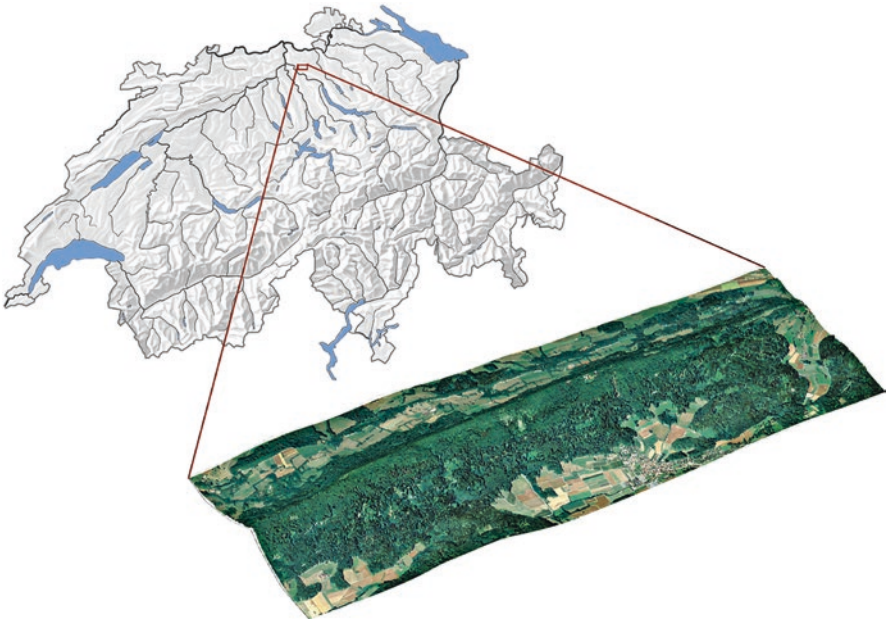

Fig. 4.2 Location of the Laegeren site within Switzerland

Norway spruce (*Picea abies (L.) Karst.*) are dominant. The forest stand has a relatively high diversity of species, ages, and diameters (Eugster et al. 2007). The ground cover mainly consists of bare soil, boulders, and litter, while the sparse understory vegetation is dominated by herbs and shrubs. Average canopy height (CH) is 24.9 m, with a maximum of 49 m, and the stem density is 270 stems per ha.

4.3 Data

4.3.1 In-Situ Data

Ground data with varying spatial, spectral, and temporal resolution allow for the 3-D reconstruction of the Laegeren, its attribution with leaf optical properties (LOPs), and generation of a reference database for parameterization and validation purposes. We used multitemporal TLS on a 60 m × 60 m plot (Sect. 4.3.2.2) and an extensive forest inventory for an area of 300 m × 300 m, which is extended to 300 m × 900 m for the simulation of EO data. In the inventory data, the type and accurate position of the trees, as well as their crown dimension and offset due to leaning stems, social position, and vertical stratification of the crown, were recorded (Sect. 4.3.1.2). In addition, the occurrence and characterization of the understory was mapped in the field and interpolated to a 2 m × 2 m grid using an ALS-based classification (Leiterer et al. 2013).

4.3.1.1 Measurements of Leaf Optical Properties

To obtain the optical properties of tree foliage, we used an integrating sphere coupled with an Analytical Spectral Devices (ASD) FieldSpec-3. Measurements of hemispherical and directional reflectance and transmittance, both from the abaxial and adaxial side of the leaves, were taken. To take into account the vertical variability of LOPs, we sampled in three different crown parts (top, middle, bottom), representing different lighting conditions in the canopy (e.g., sunlit, transitional, shaded). Deciduous leaves were collected from ten individual trees of five species (*Acer pseudoplatanus* spp., *Fagus excelsior*, *F. sylvatica*, *Ulmus glabra*, and *Tilia platyphyllos*). Measurements of aerosol optical depth (AOD) and precipitable amount of water (PAW) were provided by the aerosol robotic network (AERONET) as level 2.0 quality-assured data. For details of the sampling and measurement scheme, see Schneider et al. (2014).

4.3.1.2 Forest Inventory

An exhaustive forest inventory was carried out, individually addressing all single trees with a diameter at breast height (DBH) above 20 cm on the 300 m × 300 m site. Variables recorded for each tree included DBH, species, social status, and crown shift (i.e., an estimation of the magnitude and horizontal direction of the crown center in respect to the foot of the stem). The latter is of particular relevance on the Laegeren site because many trees have leaning stems due to topography and shallow soils. A geodetic tachymeter was used for the surveying, enabling fast and accurate electronic tree location measurements. Using all measured points, a polygonal traverse was calculated resulting in the x, y, z coordinates for each measurement position with an error range of millimeters for the TLS measurements and a maximum of 10 cm in x, y, and z for all other field measurements. The relative locations were transformed to absolute Swiss national coordinates using three differentially corrected global positioning system (GPS) base points, which were placed in canopy gaps. See Fig. 4.3 for a visualization of the tree inventory.

4.3.2 RS Data

4.3.2.1 Airborne Laser Scanning

To provide 3-D structure information across the whole study area, we relied on two airborne laser scanning campaigns, using a RIEGL LMS-Q680i scanner under leaf-on conditions and a RIEGL LMS-Q560 scanner under leaf-off conditions. Flight strips have an overlap of approximately 50%. Full-waveform features, namely, echo width and intensity, were extracted from the data using the software RiANALYZE and were assigned to the individual returns in the multiple-echo point cloud.

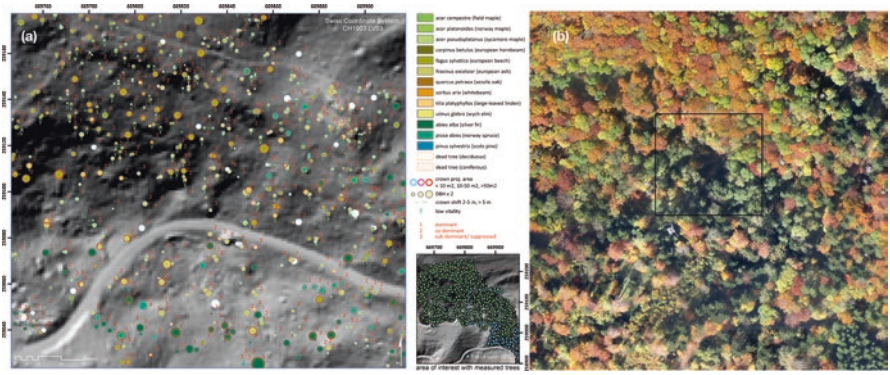

Fig. 4.3 Subset of single-tree ground inventory (**a**) and UAV-based RGB imagery acquired in fall (**b**). The black box in (**b**) denotes the subset presented in (**a**). The gray structure southwest of the bounding box is the flux tower, and the small inset shows the total extent of the single-tree ground inventory

The point cloud was filtered to classify ground and vegetation points, and the ground points were subsequently interpolated to a raster of 1 m resolution. For a detailed description of the digital terrain model (DTM) generation, see Leiterer et al. (2013). DTM accuracy was assessed using more than 500 TLS-measured road surface and bare soil points (see Sect. 4.3.2.2), which were related to the national land survey and resulted in a mean height uncertainty of about ±0.25 m. For each point of the full point cloud, the height above ground was calculated by subtracting the interpolated DTM value from the corresponding echo height above sea level, providing the vertical distance of the vegetation echoes to the terrain underneath.

4.3.2.2 Terrestrial Laser Scanning

On a subset of about 60 m × 60 m, a ground-based TLS survey was carried out using a Riegl VZ1000 instrument. A total of 40 scans on 20 scan locations were taken because each location had to be covered by two scans due to the VZ1000's camera scanning pattern (Morsdorf et al. 2018). About 50 reflective targets were placed within the scene and later used for co-registration of the scans. For co-registering RiSCAN Pro was used, and we used the ALS data to subsequently globally adjust (rotate and translate) the unified TLS point cloud. Due to the high and dense canopy, TLS needs to be complemented by laser data from above the canopy, providing more information in the upper part, either by ALS or UAV-based laser scanners. For biomass retrievals, the occlusion of upper canopy material in TLS data might be less of a problem because stems generally taper off toward the top. However, if simulation of the radiative regime and subsequent comparison with EO data gathered with a top-of-canopy perspective is the aim, TLS in denser forests needs to be complemented with laser scanning data from above the canopy (Morsdorf et al. 2017, 2018) (Fig. 4.4).

Fig. 4.4 Terrestrial laser scan of a beech-dominated part of the study area. Transect measures about 30 m (width) × 4 m (depth). One can observe a general thinning of the point cloud toward the top due to occlusion

4.3.3 Multispectral and Imaging Spectroscopy Data

Imaging spectroscopy data were acquired under clear sky conditions using the APEX imaging spectrometer (Schaepman et al. 2015). The average flight altitude was 4500 m a.s.l. resulting in an average ground pixel size of 2 m. APEX measured at-sensor radiances in 316 spectral bands ranging from 372 nm to 2540 nm. APEX data were processed to hemispherical-conical reflectance factors in the APEX processing and archiving facility (Hueni et al. 2009). Level 1 (L1) calibrated radiances were obtained by inverting the instrument model, applying coefficients established during calibration, and characterization at the APEX Calibration Home Base (CHB) in Oberpfaffenhofen, Germany. The position and orientation of each pixel in 3-D space was based on automatic geocoding in PARGE v3.269, using the swissALTI3D DTM. L1 data were then converted to hemispherical conical reflectance factors (HCRFs, Schaepman-Strub et al. 2006) by employing ATCOR4 v7.0 in the smile aware mode. The APEX data were complemented with other passive optical data of varying spatial and spectral resolution to build up an EO data set (Fig. 4.5). This EO data set enables cross-comparisons between the 3-D RT modeled and the actual, measured top-of-atmosphere (TOA) reflectance values at different spectral and spatial resolutions and thus an absolute evaluation of the 3-D reconstructed forest scenes and the RTM parameterization. The EO data acquired during the 2010–2014 growing seasons covers a variety of spectral and spatial resolutions:

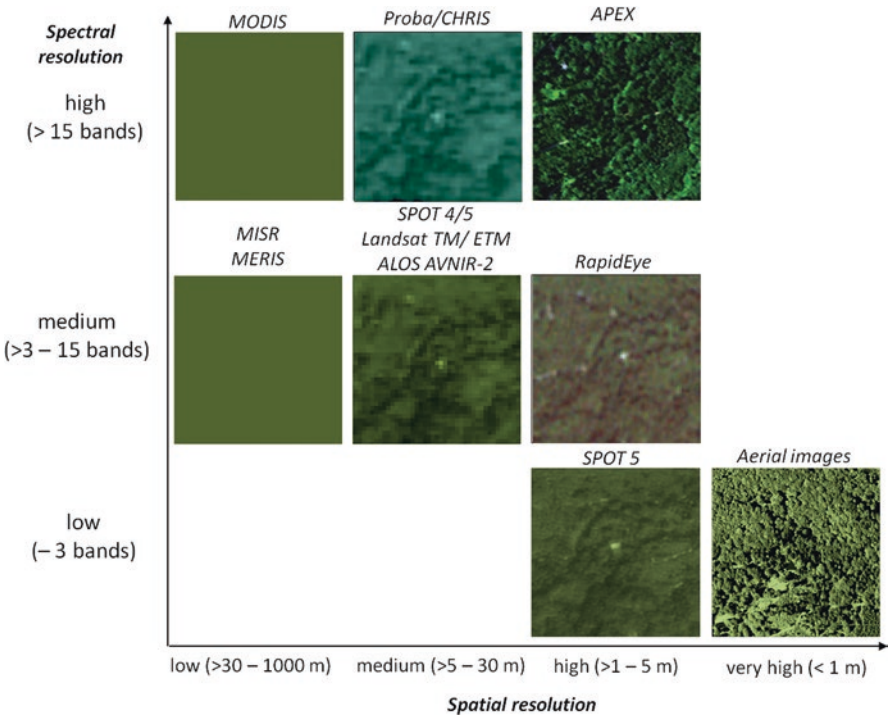

Fig. 4.5 The spatial and spectral scales covered by Earth observation (EO) data gathered for validation and up- and downscaling purposes

imaging spectrometer data from APEX (2 m × 2 m, see above for details) as well as multispectral data from RapidEye (5 m × 5 m, 4 scenes), SPOT HRG (10 m × 10 m, 5 scenes), PROBA CHRIS (17 m × 17 m, 1 scene), Landsat TM/ETM+/OLI (30 m × 30 m, 37 scenes), ENVISAT MERIS (300 m × 300 m, 8 scenes), and Aqua/Terra MODIS (250 m × 250 m, monthly). We use APEX data for the spectral validation and a RapidEye scene for the spatial validation of our 3-D RTM approach.

4.4 Methods

4.4.1 In-Situ Data Processing

4.4.1.1 Optical Properties

LOPs were calculated separately for deciduous and coniferous trees. A linear spectral forward mixing was applied to calculate the reflectance and transmittance spectra of sunlit, transitional, and shaded leaves and needles. Because the spectra

were found to match well with those in literature, the data were used directly instead of a forward simulation of a LOP model (Feret et al. 2008). This was done to reduce the number of parameters and associated uncertainties. The broadleaf species composition used for spectral mixing was derived from the forest inventory information and is dominated by beech (about 50%), with lesser contributions from maple, elm, linden, and ash.

One particular issue of the Laegeren site is its large variation in the spectral background. Because we had multitemporal full-waveform lidar data available for the Laegeren site, we used this information to classify the ground into distinct classes (gravel, litter, soil) and assigned matching spectra from our field measurements to these classes (Leiterer et al. 2013). As Schneider et al. (2014) showed, using several understory classes instead of a homogenous (black) background makes simulated top-of-canopy (TOC) and top-of-atmosphere (TOA) reflectance values more realistic.

4.4.1.2 3-D Reconstruction

Two different approaches for 3-D reconstruction of the vegetation structure were implemented and tested. The first approach relied on a single-tree identification and the second one on a direct computation of plant area index (PAI) values inside a voxel cell. Voxels are basically 3-D pixels, dividing the 3-D space into equal-sized cubes. The single-tree detection (individual tree crown, ITC) method used was based on Morsdorf et al. (2004), which derives tree location, height, and crown diameter to reconstruct the forest in 3-D based on simple geometric primitives like rotational paraboloids. However, as with most local maxima detection-based ITC methods, its performance within the mixed forest stands of the Laegeren site was suboptimal, with tree detection rates of only 50–70%. This is much lower than what can be expected for conifer forests, where rates of up to 90% can be achieved (Kaartinen et al. 2012; Wang et al. 2016). Conifers generally have conical crowns with one distinct peak (treetop), greatly facilitating their detection as local maxima in a digital surface model (DSM). The main difference between the voxel-grid and ITC approaches is the added level of semantics (Morsdorf et al. 2018) in the single-tree case, which might be relevant for some species- and individual-focused experiments (i.e., when trying to link EO-based traits with genetic information of the individual tree). If the aim of the 3-D reconstruction is an accurate simulation of the radiative regime, single-tree identification adds a layer of unnecessary complexity, so the voxel-grid approach led to better results (Schneider et al. 2014) and was subsequently used for upscaling of the trait information (Schneider et al. 2017).

4.4.1.3 Linking Field and RS Data

The perspective of forest inventory is from within or beneath the canopy and the main sampling unit is the tree, quantified as diameter at breast height (DBH). RS, on the other hand, has a top-down perspective on the canopy, and the sampling unit

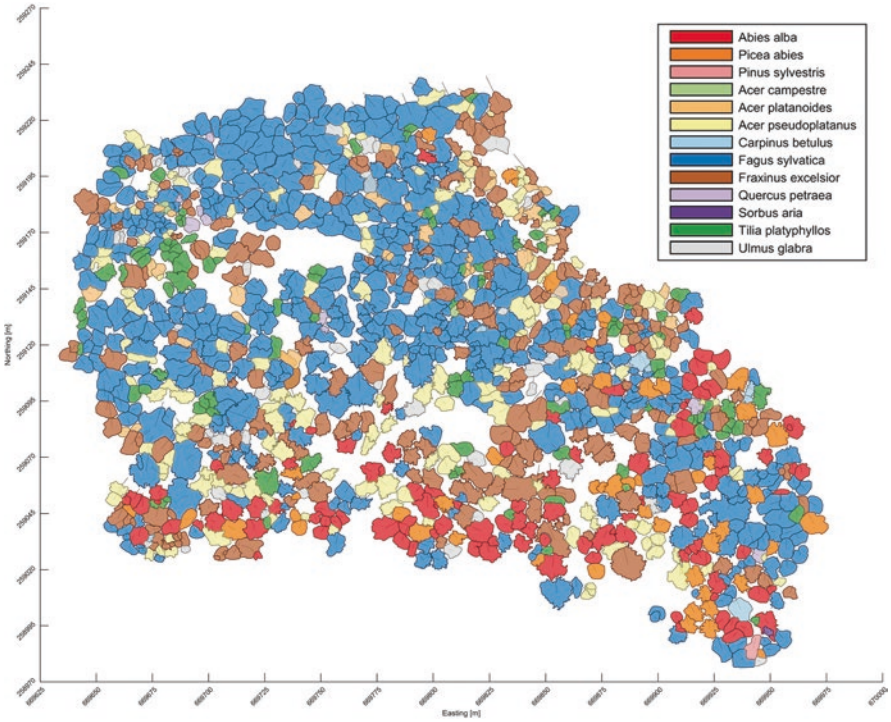

Fig. 4.6 Map of crown polygons determined from a combination of ALS and maximum leaf senescence (Fall) UAV data, linked with species information derived from the stem-referenced field inventory. Only the combination of these crown outlines and the stem map (see Fig. 4.3) allowed for individual specific computation of physiological and morphological traits

is normally a pixel. Linking these different perspectives can be difficult under any circumstances; the Laegeren site is situated on a steep slope, and trees have irregular crown shapes and different growing directions, which further complicates information matching. The first necessary step is to convert the pixel-based EO data to tree-based data by using 2-D polygons of crown boundaries. Considering the low success rates of ALS-based ITC, we manually delineated tree crowns based on UAV imagery acquired in the fall (Fig. 4.3) and matched each crown with the forest inventory data. The field inventory provided valuable additional information, such as magnitude and direction of the crown shift for trees with leaning stems, which hinders a direct stem and crown location matching based on location (Fig. 4.6).

4.4.2 Radiative Transfer Modeling

The RTM used to upscale and validate leaf-level traits such as chlorophyll and leaf water content is Discrete Anisotropic Radiative Transfer (DART; Gastellu-Etchegorry et al. 2015). Generally, a DART scene is built out of voxels with a predefined size.

To simulate vegetation such as grass or tree crowns, voxels can be filled by turbid media parameterized with PAI and leaf optical properties (LOPs). Further details of the DART model and examples of DART simulations can be found in Gastellu-Etchegorry et al. (2015). We use flux tracking in reflectance mode with the sun and the atmosphere as the only radiation sources and used DART version 5.6.0 (v739). Optical properties described in Sect. 4.4.1.1 and the forest reconstruction described in Sect. 4.4.1.2 are used to parameterize the forest canopy, background, and terrain in DART. For details of model parameterization, see Schneider et al. (2014); for details on the model-based upscaling of leaf-level traits, see Schneider et al. (2017). For the modeling results shown in Sect. 4.5.1.1, we used sun and observation angles as in the actual APEX and RapidEye acquisitions, respectively. We evaluate the performance of the combined 3-D reconstruction and RT simulation approach in two ways: spectrally, by comparing averaged simulated spectra on the core (i.e., covered by TLS measurements) site with those obtained by the APEX instrument, and, spatially, by comparing simulated bands of RapidEye over an area of 900 m × 300 m with DART-simulated reflectance at those particular wavelength regions.

4.4.3 Validation of Trait Predictions Using the RTM Approach

Three functional traits were derived from ALS data, canopy height (CH), PAI, and foliage height diversity (FHD), forming a set of morphological traits. These three were chosen because they are ecologically relevant and can be easily derived from airborne laser scanning data. Three additional functional traits—chlorophylls (CHL), carotenoids (CAR), and equivalent water thickness (EWT)—were chosen and computed using specific band ratios from the IS data (Schneider et al. 2017), forming a set of physiological traits. Both CH and CHL have been identified as primary observables for RS-EBVs, so their validation and scaling is particularly relevant. The traits were computed at a spatial aggregation unit of 6 m; for the ALS data, all echo values within a 6 m × 6 m grid cell were used for the computation, while for the IS data only sunlit pixels within the grid cell were retained for subsequent index computation. The shadow mask used for extracting sunlit pixels was derived from a DSM based on the ALS data and the solar illumination angle at the time of the IS overflight. For more details on the selected traits and their computation, please refer to Schneider et al. (2017).

The physiological traits used in this study are by definition leaf-level parameters, which need to be upscaled or averaged to be representative for the tree or canopy level. On the other hand, the morphological traits can be directly estimated from ALS data for any spatial unit. However, the chosen spatial scale and context might change how the data are interpreted (e.g., tree height needs to be estimated using single-tree information, whereas vegetation height can be derived at all different scales at the stand or plot level. See Fig. 4.7 for a map of the computed physiological and morphological traits.

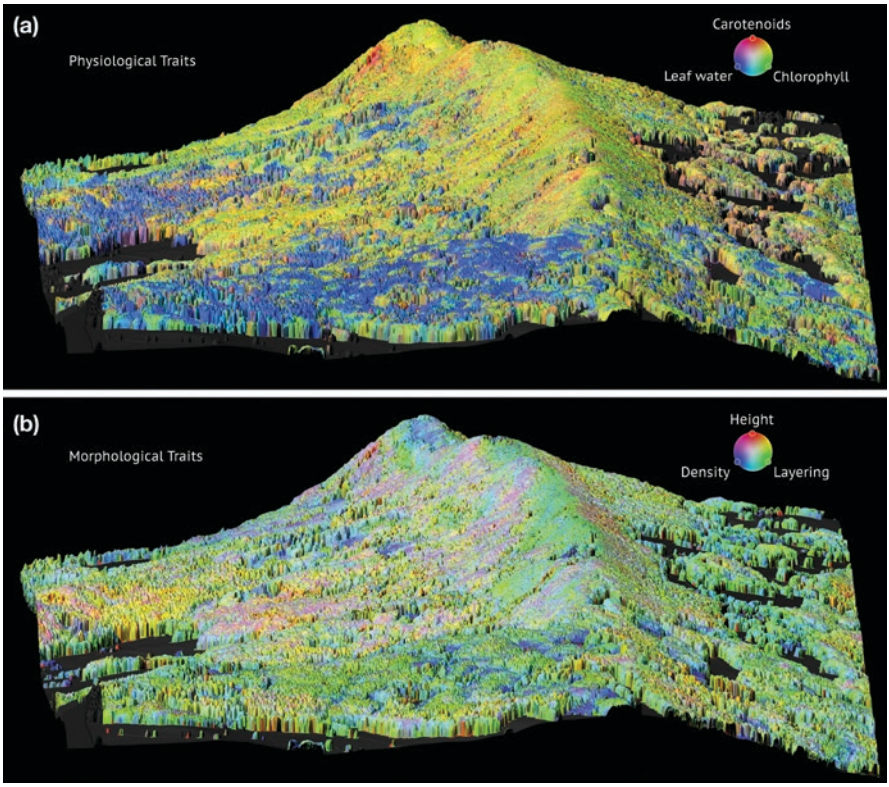

Fig. 4.7 Physiological (**a**) and morphological (**b**) traits derived from IS and ALS. For the ALS-based morphological traits, density is plant area index (PAI) and layering foliage height diversity (FHD)

4.4.4 Computation of Functional Richness

To showcase how the RTM-validated EO traits can be used for spatially explicit diversity assessments, we compute the functional richness within the 3-D trait space using a spatial subset of pixels (e.g., in a 60 m × 60 m box containing 100 pixels). In the case of the morphological traits, the 3-D trait space is spanned by the axes CH, PAI, and FHD, whereas for the physiological traits the trait space is spanned by the axes CHL, CAR, and EWT. The richness within the trait space is based on volume of a 3-D convex hull of all pixels' trait values (i.e., the larger the variation of the respective traits, the larger the volume of the convex hull). As an example, if all trait values were the same, the richness would be zero because no volume would be spanned in the 3-D trait space. Computing the richness using a pixel-based approach has the advantage of resolving both inter- and intraspecific variation of the traits,

with the latter being potentially as large as the former (e.g., as observed in our leaf spectra). For details on the definition and computation of richness and other diversity-related metrics in the scope of this work, please refer to Schneider et al. (2017).

4.5 Results and Discussion

4.5.1 Forward Simulation of Passive Optical Imagery and Comparison With EO Data

4.5.1.1 Spectral Validation

Figure 4.8 compares the spectral response of a 20 m × 20 m subplot within the Laegeren site simulated by the DART RTM with the average APEX spectrum of the same area. In contrast to Schneider et al. (2014), the improved version of the DART model used in this study shows good agreement (within the standard deviation for the 10 × 10 pixel areas) for all wavelengths, including the visible domain. The version of DART used in this study (5.6.0, v739) has a more sophisticated parameterization of the atmosphere than the older version, improving the spectral response in the visible domain (Grau and Gastellu-Etchegorry 2013; Yin et al. 2013; Gastellu-Etchegorry et al. 2015). The very good agreement of simulated and measured spectra across all bands shows that our approach of combining a 3-D reconstruction of the forest and LOPs of leaves and needles was successful in capturing the dominant scattering components of this natural system. In the near-infrared domain of the spectra, this is likely due to ALS and TLS providing accurate physical representations of 3-D canopy structure, whereas in the visible domain the quality of the LOPs

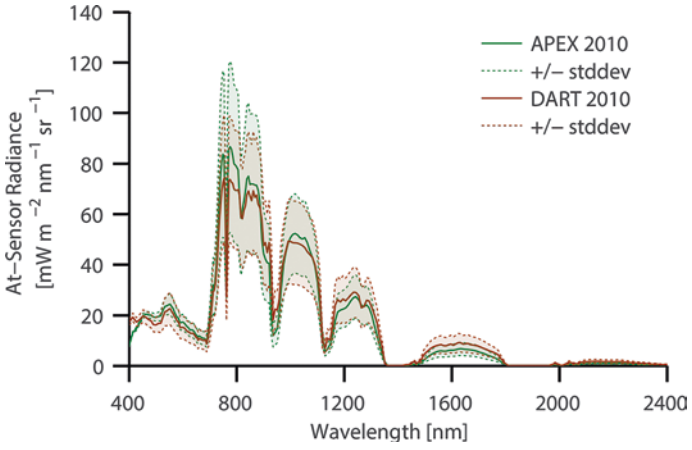

Fig. 4.8 Simulated spectral response by DART for subplot S1 in comparison with APEX data acquired over the same area. The standard deviation is computed from the single pixels in the 20 m × 20 m plot

and the representation of the atmosphere are contributing more to this excellent result. Thus, we have shown that the measured physiological trait variation at leaf level can be upscaled to canopy level (as observed by IS instruments). We used this to forward validate IS-derived physiological traits that are the basis of the functional richness computation in Sect. 4.5.2. This RTM-based link is a key component of our validation framework because typically field-measured spectra and the traits based on spectral indices cannot be assumed to be representative for the respective signals measured at the imaging sensor above the canopy.

4.5.1.2 Spatial Validation

Figure 4.9 shows a comparison of the spatial patterns in both simulated and actual RapidEye imagery obtained over the Laegeren site in leaf-on conditions. When subsampled to the 5 m resolution of RapidEye, our approach produces very similar spatial patterns, properly resolving shadows and highlights due to forest structure and underlying topography effectively contained in the ALS data and transferred to

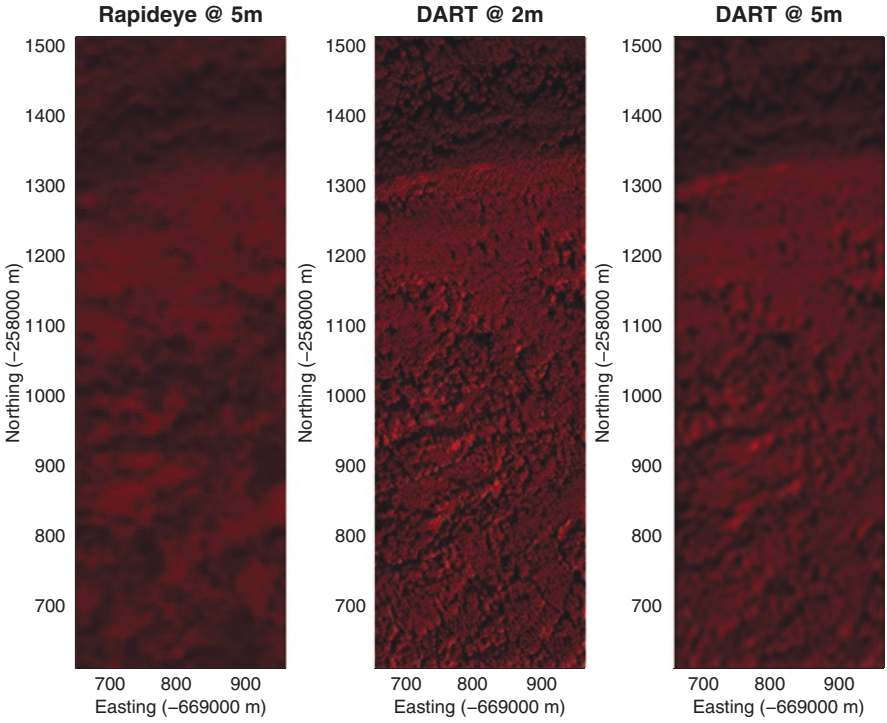

Fig. 4.9 RGB false-color composite using the RapidEye bands 5 (R), 3 (G), and (2), both for the simulated image using DART (center panel) and actual RapidEye data acquired over the site (left panel). The right panel shows a smoothed version of the DART simulation to accommodate for the lower resolution (5 m) of the RapidEye imaging sensor

the RT model by the PAI voxel grid. If LOPs can be assumed to be uniform across a site or region, the presented approach can be used for larger areas, only relying on ALS data to parameterize the RT model and using the LOPs measured at a subset of the site or taken from spectral libraries. ALS data are generally available at regional and national scales, effectively bridging the gap between point-based field inventories and global scale satellite imagery. Using such larger-scale simulated EO data, retrieval methods for RS-EBV primary observables such as CHL and vegetation height can be tested and validated. The 3-D simulation environment we established explicitly or implicitly contains all these variables in an easily retrievable format.

4.5.2 Functional Diversity of Laegeren Site

Figure 4.10 shows the spatial distribution of the richness as computed from the three morphological and physiological traits. The most prominent pattern is the strong topographic effect of the Laegeren mountain ridge, which is equally present in both

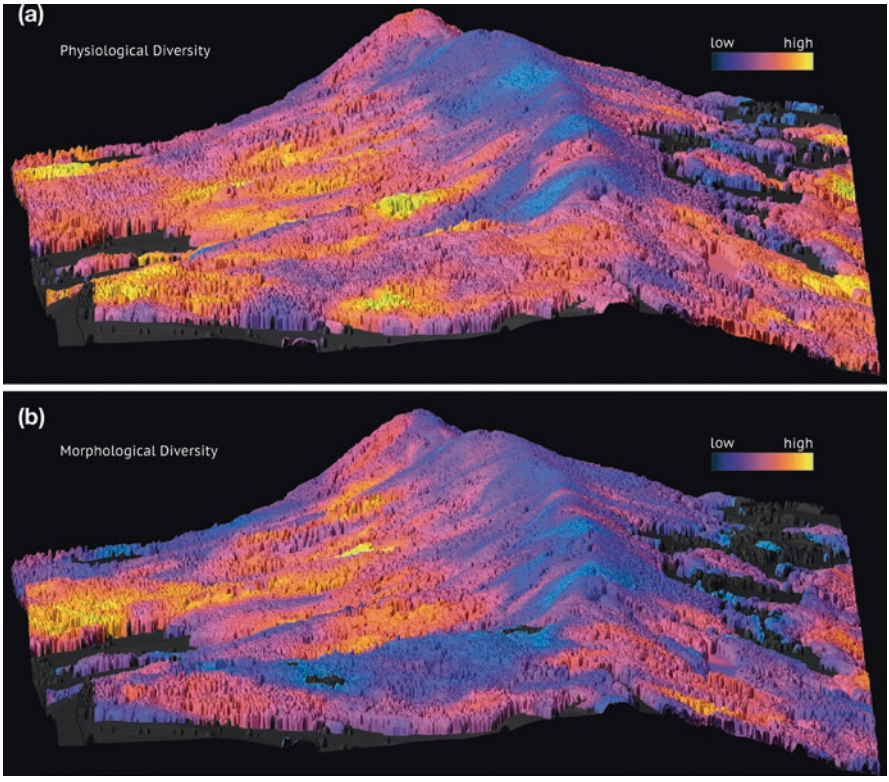

Fig. 4.10 Physiological (**a**) and morphological (**b**) richness determined within the trait space spanned by three traits

richness maps. The ridge and the associated steep slopes affect many environmental variables, which could act as filter for niche space and thus diversity. Higher altitude is linked with decreased temperature, whereas the slope is contributing to lesser soil depths and water availability and increased incoming radiation, at least for the part south of the ridge. Thus, the environmental conditions are harsher close to the ridge, which might explain the decrease of functional richness we observe in this context. In the lower regions, morphological and physiological richness exhibit differing spatial patterns. We assume that changes of the morphological richness in lower parts parallel to ridge are caused by the different stand management regimes and associated stand ages and structures. For the physiological richness, differences in species composition seem to be a dominant effect, with the conifer-dominated stands having a lower functional richness and the old-growth mixed stands being functionally richer.

4.6 Conclusion and Outlook

Modern RS technologies increasingly face a validation paradox—i.e., it is very difficult to provide ground-based validation data that match the spatial (resolution and extent), temporal, and thematic characteristics of modern EO data sets. As an example, ALS-derived tree height is assumed to be more accurate than field measurements, but it cannot be proved using field data alone. By using laser scanning-derived 3-D structure together with LOPs in an RT model approach, we have shown a way to overcome such mismatches and provide a framework that could be established across a range of sites around the globe to prototype and validate EO-based data and products in the future. Such a forward validation will as well pave the way for products that are not measurable in the field, but still might be relevant in the context of ecosystem function and diversity. The RTM approach provides a physical and mechanistic way to learn about the information content of EO data, and a combination of this approach with recent developments in the machine learning domain could provide interesting perspectives.

With the trait-based functional richness assessment, we demonstrated how a spatially extended monitoring using the complementary technologies imaging spectroscopy and lidar would work and what kind of insights into ecosystem functioning it could generate. In addition, the trait maps and the derived functional richness could be used for spatiotemporal gap filling of in-situ observational networks such as the global forest biodiversity initiative, complementing the diversity information that these provide.

In the future, these data streams in conjunction with the EBV concept (Fernández et al., Chap. 18) will give policy-makers around the world useful tools to assess and report on the biodiversity. To speed up this process, the European Space Agency funded the GlobDiversity project starting in 2017 in the tradition of similar projects for some of the essential climate variables. The project's goal is to demonstrate the capability and utility of producing a set of selected RS-EBV data sets in different

regions and biomes around the globe and with high spatial resolution (10–30 m) using the newest-generation satellite data, such as Sentinel-2 and Landsat 8. In addition, the project shall suggest in a reference document how to describe RS-EBVs and how they could be engineered and validated. We believe that the 3-D reconstruction and RT modeling approach highlighted in this chapter could be applied across a global range of sites to fulfill this task.

Acknowledgments The contributions of F.M., F.D.S., and M.E.S. are supported by the University of Zurich Research Priority Program on Global Change and Biodiversity, and the contribution of D.K. was with support from the European Union's 7th Framework Program (FP7/ 2014–2018) under EUFAR2 contract no. 312609.

References

Asner GP, Warner AS (2003) Canopy shadow in ikonos satellite observations of tropical forests and savannas of. Environment 87(4):521–533

Bar-On YM, Phillips R, Milo R (2018) The biomass distribution on earth. Proc Natl Acad Sci 115(25):6506

Chapin FS III, Zavaleta ES, Eviner VT, Naylor RL, Vitousek PM, Reynolds HL, Hooper DU, Lavorel S, Sala OE, Hobbie SE, Mack MC, Dıaz S (2000) Consequences of changing biodiversity. Nature 405(6783):234–242

Chave J, Réjou-Méchain M, Burquez A, Chidumayo E, Colgan MS, Delitti WB, Duque A, Eid T, Fearnside PM, Goodman RC, Henry M, Martínez-Yrízar A, Mugasha WA, Muller-Landau HC, Mencuccini M, Nelson BW, Ngomanda A, Nogueira EM, Ortiz-Malavassi E, Pelissier R, Ploton P, Ryan CM, Saldarriaga JG, Vieilledent G (2014) Improved allometric models to estimate the aboveground biomass of tropical trees. Glob Chang Biol 20(10):3177–3190

Cote JF, Widlowski JL, Fournier RA, Verstraete MM (2009) The structural and radiative consistency of three-dimensional tree reconstructions from terrestrial lidar. Remote Sens Environ 113(5):1067–1081

Disney M, Lewis P, Saich P (2006) 3d modeling of forest canopy structure for remote sensing simulations in the optical and microwave domains. Remote Sens Environ 100(1):114–132

Eugster W, Zeyer K, Zeeman M, Michna P, Zingg A, Buchmann N, Emmeneg- ger L (2007) Nitrous oxide net exchange in a beech dominated mixed forest in Switzerland measured with a quantum cascade laser spectrometer. Biogeosci Discuss 4:1167–1200

Feret JB, Francois C, Asner GP, Gitelson AA, Martin RE, Bidel LP, Ustin SL, le Maire G, Jacquemoud S (2008) Prospect-4 and 5: advances in the leaf optical properties model separating photosynthetic pigments. Remote Sens Environ 112(6):3030–3043

Gardner T (2010) Monitoring forest biodiversity: improving conservation through ecologically responsible management, vol 9781849775106. Earthscan, London

Gastellu-Etchegorry J, Zagolski F, Romier J (1996) A simple anisotropic reflectance model for homogeneous multilayer canopies. Remote Sens Environ 57(1):22–38

Gastellu-Etchegorry JP, Yin T, Lauret N, Cajgfinger T, Gregoire T, Grau E, Feret JB, Lopes M, Guilleux J, Dedieu G, Malenovský Z, Cook BD, Morton D, Rubio J, Durrieu S, Cazanave G, Martin E, Ristorcelli T (2015) Discrete anisotropic radiative transfer (DART 5) for modeling airborne and satellite spectroradiometer and lidar acquisitions of natural and urban landscapes. Remote Sens 7(2):1667–1701

Grau E, Gastellu-Etchegorry JP (2013) Radiative transfer modeling in the earth-atmosphere system with {DART} model. Remote Sens Environ 139:149–170

Hansen MC, Potapov PV, Moore R, Hancher M, Turubanova SA, Tyukavina A, Thau D, Stehman SV, Goetz SJ, Loveland TR, Kommareddy A, Egorov A, Chini L, Justice CO, Townshend JRG (2013) High-resolution global maps of 21st-century forest cover change. Science 342(6160):850–853

Hilker T, Coops NC, Hall FG, Black TA, Wulder MA, Nesic Z, Krishnan P (2008) Separating physiologically and directionally induced changes in pri using brdf models. Remote Sens Environ 112(6):2777–2788

Homolov́a L, Malenovský Z, Clevers JGPW, Garćıa-Santos G, Schaepman ME (2013) Review of optical-based remote sensing for plant trait mapping. Ecol Complex 15:1–16

Huemmrich KF (2001) The geosail model: a simple addition to the sail model to describe discontinuous canopy reflectance. Remote Sens Environ 75(3):423–431

Hueni A, Biesemans J, Meuleman K, Dell'Endice F, Schlapfer D, Odermatt D, Kneubuehler M, Adriaensen S, Kempenaers S, Nieke J, Itten K (2009) Structure, components, and interfaces of the airborne prism experiment (apex) processing and archiving facility. IEEE Trans Geosci Remote Sens 47(1):29–43

Hyyppa J, Kelle O, Lehikoinen M, Inkinen M (2001) A segmentation-based method to retrieve stem volume estimates from 3-d tree height models produced by laser scanners. IEEE Trans Geosci Remote Sens 39:969–975

Isbell F, Gonzalez A, Loreau M, Cowles J, Dıaz S, Hector A, Mace GM, Wardle DA, O'Connor MI, Duffy JE, Turnbull LA, Thompson PL, Larigauderie A (2017) Linking the influence and dependence of people on biodiversity across scales. Nature 546:65–72

Jacquemoud S (1993) Inversion of the prospect + sail canopy reflectance model from aviris equivalent spectra: theoretical study. Remote Sens Environ 44(2–3):281–292

Jacquemoud S, Baret F (1990) Prospect: a model of leaf optical properties spectra. Remote Sens Environ 34(2):75–91

Jetz W, Cavender-Bares J, Pavlick R, Schimel D, Davis F, Asner G, Guralnick R, Kattge J, Latimer A, Moorcroft P, Schaepman M, Schildhauer M, Schneider F, Schrodt F, Stahl U, Ustin S (2016) Monitoring plant functional diversity from space. Nat Plants 2(3):16024

Kaartinen H, Hyyppa J, Yu X, Vastaranta M, Hyyppa H, Kukko A, Holopainen M, Heipke C, Hirschmugl M, Morsdorf F, Næsset E, Pitkanen J, Popescu S, Solberg S, Wolf BM, Wu JC (2012) An international comparison of individual tree detection and extraction using airborne laser scanning. Remote Sens 4:950–974

Knyazikhin Y, Lewis P, Disney MI, Mottus M, Rautiainen M, Stenberg P, Kaufmann RK, Marshak A, Schull MA, Latorre Carmona P, Vanderbilt V, Davis AB, Baret F, Jacquemoud S, Lyapustin A, Yang Y, Myneni RB (2013) Reply to Ollinger et al.: remote sensing of leaf nitrogen and emergent ecosystem properties. Proc Natl Acad Sci 110(27):E2438

Kotz B, Schaepman M, Morsdorf F, Bowyer P, Itten K, Allg̈ower B (2004) Radiative transfer modeling within a heterogeneous canopy for estimation of forest fire fuel properties. Remote Sens Environ 92(3):332–344

Lefsky MA, Cohen WB, Acker SA, Parker GG, Spies TA, Harding D (1999) Lidar remote sensing of the canopy structure and biophysical properties of Douglas-fir western hemlock forests. Remote Sens Environ 70:339–361

Leiterer R, Mücke W, Morsdorf F, Hollaus M, Pfeifer N, Schaepman M (2013) Operational forest structure monitoring using airborne laser scanning. Photogrammetrie Fernerkundung Geoinformation 3:173–184

Lewis P, Disney M (2007) Spectral invariants and scattering across multiple scales from within-leaf to canopy. Remote Sens Environ 109(2):196–206

Meroni M, Colombo R, Panigada C (2004) Inversion of a radiative transfer model with hyperspectral observations for LAI mapping in poplar plantations. Remote Sens Environ 92(2):195–206

Morsdorf F, Meier E, Kotz B, Itten KI, Dobbertin M, Allgower B (2004) Lidar-based geometric reconstruction of boreal type forest stands at single tree level for forest and wildland fire management. Remote Sens Environ 92(3):353–362, forest Fire Prevention and Assessment

Morsdorf F, Kotz B, Meier E, Itten K, Allgower B (2006) Estimation of LAI and fractional cover from small footprint airborne laser scanning data based on gap fraction. Remote Sens Environ 104(1):50–61

Morsdorf F, Marell A, Koetz B, Cassagne N, Pimont F, Rigolot E, Allgower B (2010) Discrimination of vegetation strata in a multi-layered mediterranean forest ecosystem using height and intensity information derived from airborne laser scanning. Remote Sens Environ 114(7):1403–1415

Morsdorf F, Eck C, Zgraggen C, Imbach B, Schneider F, Kükenbrink D (2017) UAV-based LiDAR acquisition for the derivation of high-resolution forest and ground information. Lead Edge 36(7):566–570

Morsdorf F, Kükenbrink D, Schneider FD, Abegg M, Schaepman ME (2018) Close-range laser scanning in forests: towards physically based semantics across scales. Interface Focus 8(2):20170046

Myneni R, Nemani R, Running S (1997) Estimation of global leaf area index and absorbed PAR using radiative transfer models. IEEE Trans Geosci Remote Sens 35:1380–1393

Myneni RB, Maggion S, Iaquinta J, Privette JL, Gobron N, Pinty B, Kimes DS, Verstraete MM, Williams DL (1995) Optical remote sensing of vegetation: Modeling, caveats, and algorithms. Remote Sens Environ 51(1):169–188

Næsset E (2002) Predicting forest stand characteristics with airborne scanning laser using a practical two-stage procedure and field data. Remote Sens Environ 80(1):88–99

Nelson R (1997) Modeling forest canopy heights: the effects of canopy shape. Remote Sens Environ 60:327–334

Nelson R (2013) How did we get here? An early history of forestry lidar. Can J Remote Sens 39(s1):S6–S17

Ni W, Li X, Woodcock C, Caetano M, Strahler A (1999) An analytical hybrid gort model for bidirectional reflectance over discontinuous plant canopies. IEEE Trans Geosci Remote Sens 37:987–999

Niinemets Ü, Kull O, Tenhunen J (1998) An analysis of light effects on foliar morphology, physiology, and light interception in temperate deciduous woody species of contrasting shade tolerance. Tree Physiol 18(10):681–696

North P (1996) Three-dimensional forest light interaction model using a monte carlo method. IEEE Trans Geosci Remote Sens 34(4):946–956

O'Connor B, Secades C, Penner J, Sonnenschein R, Skidmore A, Burgess ND, Hutton JM (2015) Earth observation as a tool for tracking progress towards the aichi biodiversity targets. Remote Sens Ecol Conserv 1(1):19–28

Parmesan C, Yohe G (2003) A globally coherent fingerprint of climate change impacts across natural systems. Nature 421(6918):37–42

Pereira H, Ferrier S, Walters M, Geller G, Jongman R, Scholes R, Bruford M, Brummitt N, Butchart S, Cardoso A, Coops N, Dulloo E, Faith D, Freyhof J, Gregory R, Heip C, Hoft R, Hurtt G, Jetz W, Karp D, McGeoch M, Obura D, Onoda Y, Pettorelli N, Reyers B, Sayre R, Scharlemann J, Stuart S, Turak E, Walpole M, Wegmann M (2013) Essential biodiversity variables. Science 339(6117):277–278

Pettorelli N, Wegmann M, Skidmore A, Mücher S, Dawson T, Fernandez M, Lucas R, Schaepman M, Wang T, O'Connor B, Jongman R, Kempeneers P, Sonnenschein R, Leidner A, Bohm M, He K, Nagendra H, Dubois G, Fatoyinbo T, Hansen M, Paganini M, de Klerk H, Asner G, Kerr J, Estes A, Schmeller D, Heiden U, Rocchini D, Pereira H, Turak E, Fernandez N, Lausch A, Cho M, Alcaraz-Segura D, McGeoch M, Turner W, Mueller A, St-Louis V, Penner J, Vihervaara P, Belward A, Reyers B, Geller G (2016) Framing the concept of satellite remote sensing essential biodiversity variables: challenges and future directions. Remote Sensing in Ecology and Conservation 2(3):122–131

Popescu SC, Wynne RH, Nelson RF (2002) Estimating plot-level tree heights with lidar: local filtering with a canopy-height based variable window size. Comput Electron Agric 37(1–3):71–95

Raumonen P, Kaasalainen M, Akerblom M, Kaasalainen S, Kaartinen H, Vastaranta M, Holopainen M, Disney M, Lewis P (2013) Fast automatic precision tree models from terrestrial laser scanner data. Remote Sens 5(2):491

Running S, Nemani R, Heinsch F, Zhao M, Reeves M, Hashimoto H (2004) A continuous satellite-derived measure of global terrestrial primary production. Bioscience 54(6):547–560

Schaepman ME, Ustin SL, Plaza AJ, Painter TH, Verrelst J, Liang S (2009) Earth system science related imaging spectroscopy - an assessment. Remote Sens Environ 113(Suppl. 1):S123–S137

Schaepman ME, Jehle M, Hueni A, D'Odorico P, Damm A, Weyermann J, Schnei- d FD, Laurent V, Popp C, Seidel FC, Lenhard K, Gege P, Küchler C, Brazile J, Kohler P, Vos LD, Meuleman K, Meynart R, Schlapfer D, Kneubühler M, Itten KI (2015) Advanced radiometry measurements and earth science applications with the airborne prism experiment (apex). Remote Sens Environ 158:207–219

Schaepman-Strub G, Schaepman M, Painter T, Dangel S, Martonchik J (2006) Reflectance quantities in optical remote sensing–definitions and case studies. Remote Sens Environ 103(1):27–42

Schneider FD, Leiterer R, Morsdorf F, Gastellu-Etchegorry JP, Lauret N, Pfeifer N, Schaepman ME (2014) Simulating imaging spectrometer data: 3d forest modeling based on lidar and in situ data. Remote Sens Environ 152:235–250

Schneider FD, Morsdorf F, Schmid B, Petchey OL, Hueni A, Schimel DS, Schaepman ME (2017) Mapping functional diversity from remotely sensed morphological and physiological forest traits. Nat Commun 8(1):1441

Skidmore A, Pettorelli N, Coops N, Geller G, Hansen M, Lucas R, Mücher C, O'Connor B, Paganini M, Pereira H, Schaepman M, Turner W, Wang T, Weg- mann M (2015) Environmental science: agree on biodiversity metrics to track from space. Nature 523(7561):403–405

Turner M (1989) Landscape ecology: the effect of pattern on process. Annu Rev Ecol Syst 20:171–197

Verhoef W, Bach H (2007) Coupled soil-leaf-canopy and atmosphere radiative transfer modeling to simulate hyperspectral multi-angular surface reflectance and {TOA} radiance data. Remote Sens Environ 109(2):166–182

Wang Y, Hyyppa J, Liang X, Kaartinen H, Yu X, Lindberg E, Holmgren J, Qin Y, Mallet C, Ferraz A, Torabzadeh H, Morsdorf F, Zhu L, Liu J, Alho P (2016) International benchmarking of the individual tree detection methods for modeling 3-d canopy structure for silviculture and forest ecology using airborne laser scanning. IEEE Trans Geosci Remote Sens 54(9):5011–5027

Widlowski JL, Robustelli M, Disney M, Gastellu-Etchegorry JP, Lavergne T, Lewis P, North P, Pinty B, Thompson R, Verstraete M (2008) The rami online model checker (romc): a web-based benchmarking facility for canopy reflectance models. Remote Sens Environ 112(3):1144–1150

Widlowski JL, Mio C, Disney M, Adams J, Andredakis I, Atzberger C, Brennan J, Busetto L, Chelle M, Ceccherini G, Colombo R, Cote JF, Eenmae A, Essery R, Gastellu-Etchegorry JP, Gobron N, Grau E, Haverd V, Homolova L, Huang H, Hunt L, Kobayashi H, Koetz B, Kuusk A, Kuusk J, Lang M, Lewis PE, Lovell JL, Malenovsky Z, Meroni M, Morsdorf F, Mottus M, Ni-Meister W, Pinty B, Rautiainen M, Schlerf M, Somers B, Stuckens J, Verstraete MM, Yang W, Zhao F, Zenone T (2015) The fourth phase of the radiative transfer model intercomparison (rami) exercise: actual canopy scenarios and conformity testing. Remote Sens Environ 169:418–437

Wilson J, Peet R, Dengler J, Partel M (2012) Plant species richness: the world records. J Veg Sci 23(4):796–802

Wulder M, Coops N, Hudak A, Morsdorf F, Nelson R, Newnham G, Vastaranta M (2013) Status and prospects for lidar remote sensing of forested ecosystems. Can J Remote Sens 39(s1):S1–S5

Wulder MA, White JC, Nelson RF, Næsset E, Orka HO, Coops NC, Hilker T, Bater CW, Gobakken T (2012) Lidar sampling for large-area forest characterization: a review. Remote Sens Environ 121:196–209

Yin T, Gastellu-Etchegorry JP, Lauret N, Grau E, Rubio J (2013) A new approach of direction discretization and oversampling for 3d anisotropic radiative transfer modeling. Remote Sens Environ 135:213–223